ACS NANO

Controlling Stiction in Nano-Electro-Mechanical Systems Using Liquid Crystals

Oleksandr Buchnev,[†] Nina Podoliak,[†] Thomas Frank,[†,‡] Malgosia Kaczmarek,[‡] Liudi Jiang,[§] and Vassili A. Fedotov*,[†]

[†]Optoelectronics Research Centre and Centre for Photonic Metamaterials, [‡]Physics and Astronomy, and [§]Faculty of Engineering and the Environment, University of Southampton, Southampton, SO17 1BJ, U.K.

Ⓢ *Supporting Information*

ABSTRACT: Stiction is one of the major reliability issues limiting practical application of nano-electro-mechanical systems (NEMS), an emerging device technology that exploits mechanical movements on the scale of an integrated electronic circuit. We report on a discovery that stiction can be eliminated by infiltrating NEMS with nematic liquid crystals. We demonstrate this experimentally using a NEMS-based tunable photonic metamaterial, where reliable switching of optical response was achieved for the entire range of nanoscopic structural displacements admitted by the metamaterial design. Being a more straightforward and easy-to-implement alternative to the existing antistiction solutions, our approach also introduces an active mechanism of stiction control, which enables toggling between stiction-free and the usual (stiction-limited) regimes of NEMS operation. It is expected to greatly expand the functionality of electro-mechanical devices and enable the development of adaptive and smart nanosystems.

Liquid crystal

NEMS (reconfigurable photonic metamaterial)

KEYWORDS: *stiction, liquid crystals, reconfigurable metamaterials, NEMS, MEMS*
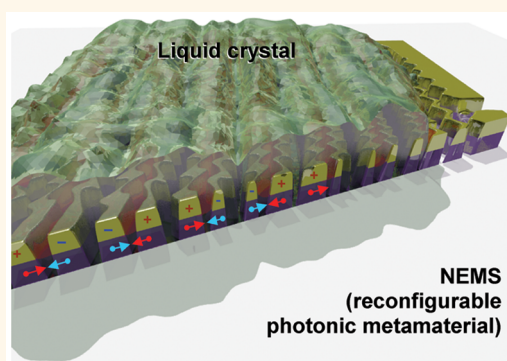
Nano-electro-mechanical systems (NEMS) are integrated miniature devices that combine electrical and mechanical components at the nanoscale. They have demonstrated great potential for a wide range of applications including nanoactuators and sensors,[1−3] electromagnetic detectors and quantum transducers,[4−6] low-power electronic/optical switches and relays,[7−9] memory,[10−12] and, recently, reconfigurable metamaterials and plasmonic devices.[13−17] The advancement of NEMS technology, however, is hampered by reliability issues such as "stiction", unintentional adhesion between compliant surfaces of the mechanical components, which leads to their permanent damage.[18,19]

Stiction occurs when surface adhesion forces such as capillary, van der Waals, or electrostatic forces (as well as their combinations) are stronger than the mechanical restoring force exhibited by an actuator. Although stiction can normally be prevented at the device fabrication stage by changing the surface hydrophobicity or by eliminating liquid−vapor interfaces through supercritical fluid, freeze-drying, or dry-release methods,[20−22] failure may still arise due to changes in ambient conditions or during routine operation of the device when its mechanical components come into close contact with each other. Currently employed methods of tackling stiction include surface treatment and coatings[23−25] and tailoring the designs of cantilevers and contact electrodes.[26,27] Being recognized as the major problem in microscale electro-

mechanical systems (MEMS),[18,28] stiction has an even higher impact on the reliability of NEMS, which are characterized by substantially larger surface-to-volume ratio. In the latter case, however, the application of stiction-preventive measures that have been found effective for MEMS[24,29−31] is quite challenging given the scale of NEMS devices.

Here we show that infiltrating NEMS with nematic liquid crystals (as illustrated in Figure 1a) yields a simple, yet efficient, alternative to the existing antistiction solutions and enables robust control of nanoscopic actuations in NEMS for the entire range of physically allowed displacements. Our approach also enables on-demand, fully reversible transition between stiction-free and stiction-limited regimes of NEMS operation, which could greatly expand the functionality of the integrated electro-mechanical systems.

RESULTS AND DISCUSSION

In the reported study NEMS was represented by a reconfigurable planar metamaterial (metasurface), a nano-patterned thin metal film with a diffraction-free resonant response that can be tuned mechanically, *via* electrically
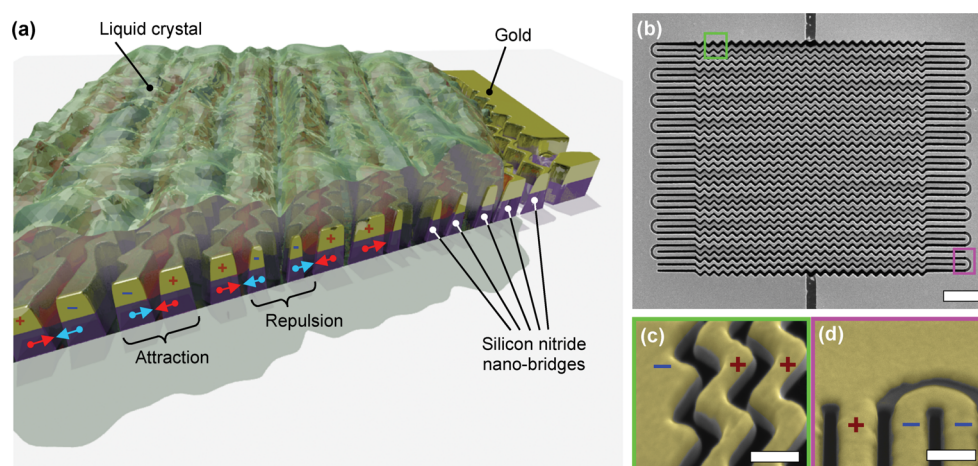
Figure 1. Nano-electro-mechanical system under study. (a) Artistic impression of a mechanically reconfigurable zigzag metasurface (cross-section) infiltrated with a liquid crystal. Red and blue arrows indicate the directions of electrically induced displacements for the nanobridges baring opposite potentials. (b) SEM image of the fabricated metasurface. Scale bar corresponds to 2 μm. (c and d) Close-up view of the areas marked in panel (b) with green and purple boxes, respectively. Images were taken with SEM at 52° to the normal and color-coded to enhance the contrast between gold (yellow) and silicon nitride (gray). Scale bar corresponds to 300 nm. Symbols "+" and "−" indicate the sign of the electrical potential applied to the corresponding wires.
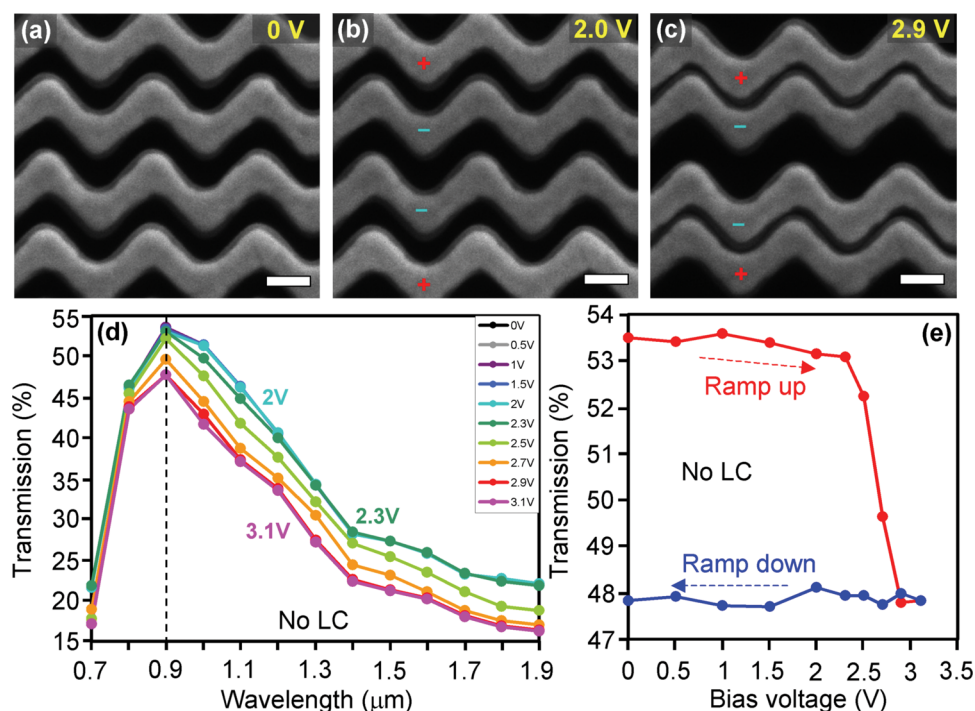

Figure 2. Irreversible electro-mechanical switching of a reconfigurable metasurface. (a−c) SEM images of a fragment of the metamaterial wire grid captured at 0 V (a), 2.0 V (b), and 2.7 V (c) in the course of electro-mechanical switching. Scale bar corresponds to 200 nm. Symbols "+" and "−" indicate the sign of the electrical potential applied to the corresponding wires. (d) Transmission spectrum of the metasurface acquired at different bias voltages during the first voltage ramp up in the range 0−3.1 V. Dashed line marks the position of the metamaterial resonance at 0 V. (d) Transmission of the metasurface measured at the resonance wavelength (0.9 μm) while ramping bias voltage up and down for the first time.

induced displacements in the fabric of the structure.[32] Our choice of this particular type of NEMS was determined by the convenience of detecting nanoscopic structural displacements, which for a metamaterial can be done optically, by observing modifications of its transmission spectra. Our metamaterial was based on a periodic array of connected V-shaped metallic nanoresonators, a tried-and-tested design[33−35] that resembles a continuous "zigzag" wire grid (see Figure 1a and b). The grid (gold) was attached to, and fully rested on, an array of dielectric

nanobridges (silicon nitride). The nanobridges had the same shape and width as the wires of the grid (Figure 1c) and could mechanically flex in the plane of the array. To reduce the stiffness of the metamaterial structure, its zigzag sections received straight extensions at both ends (see Figure 1b). Adjacent wires were electrically grouped into pairs in an alternating fashion, such that odd and even pairs were disconnected from the opposite sides of the gold frame, as shown in Figure 1d. Those modifications of the design allowed
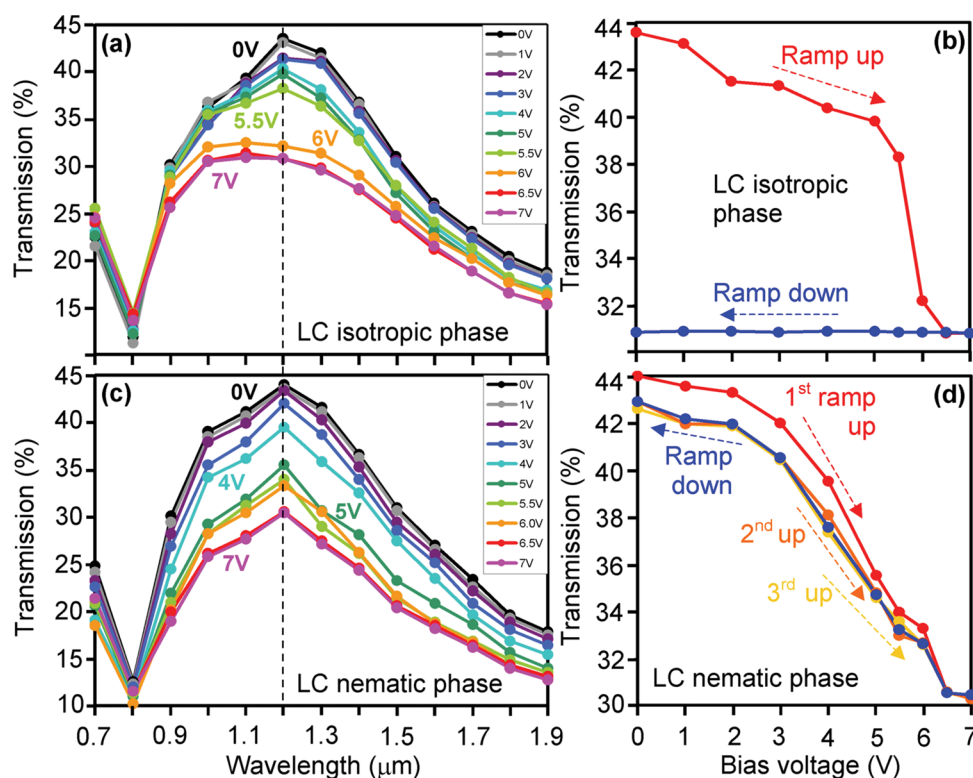
Figure 3. Switching behavior of a reconfigurable metasurface infiltrated with a liquid crystal. (a and c) Transmission spectrum of the metasurface measured at different bias voltages during the first voltage ramp up in the range 0−7 V while maintaining the liquid crystal in isotropic (a) and nematic (c) states, respectively. Dashed lines mark the position of the metamaterial resonance at 0 V. (b and d) Transmission of the metasurface measured for correspondingly isotropic and nematic states of the liquid crystal at the resonance wavelength (1.2 μm) while ramping the bias voltage up and down.

us to apply a potential difference between the pairs and induce uniform lateral displacements of the zigzag sections *via* the combination of electrostatic attraction and repulsion between the wires, as illustrated in Figure 1a. Overall, the metamaterial structure was configured to operate in the near-IR, exhibiting a plasmonic resonance as a peak in the transmission spectrum at around 0.9 μm (see Figure 2d).

The failure of the reconfigurable metamaterial due to stiction was first observed directly under a scanning electron microscope (Figure 2a−c; for videos see the Supporting Information). The nanobridges that bore the wires connected to opposite potentials came into physical contact with each other at V_p = 2.7 V (*pull-in voltage*) and remained stuck upon withdrawal of the voltage. That permanently transformed the pattern of the metamaterial from a single- to a double-wire zigzag grid (Figure 2c), which was also detected optically as an irreversible change in the transmission spectrum of a pristine metamaterial sample (see Figure 2d and e). In particular, with the potential difference ramping from 0 to 2.9 V for the first time the level of transmission at the resonance was seen to decrease from about 53% to 48%, falling sharply between 2.3 and 2.9 V. The level of transmission remained unchanged when we increased the bias voltage further, past 2.9 V, and then ramped it down to 0 V (see Figure 2e).

Similar behavior was observed for a pristine metamaterial sample infiltrated with a liquid crystal (LC) in the isotropic phase, namely, kept above the clearing temperature. The main difference was that the presence of the LC shifted the metamaterial resonance by about 0.3 μm toward the IR and marginally affected the overall transparency of the sample,

which exhibited permanent switching from 43% to 30% (see Figure 3a and b). Also, a local increase of electric permittivity caused by the presence of the LC had affected the pull-in voltage range, which shifted to higher values with the lower and upper bounds being 5.0 and 6.5 V (V_p ≈ 5.8 V). Once the potential difference exceeded 6.5 V, the transmission spectrum would not change, regardless of the bias applied thereafter, signifying mechanical damage of the reconfigurable structure.

The situation changed dramatically when we cooled the apparently damaged, LC-infiltrated sample to room temperature, thus forcing the transition of the LC from the isotropic to the nematic phase. First, upon lowering the temperature at 0 V, the transmission spectrum seemed to recover to its initial state, as had been observed just after the infiltration of the metamaterial (Figure 3c). A minor change is attributed to the optical anisotropy of LC, which in our case was relatively week and expected to result in a spectral shift of less than 3% (see Supporting Information). Next, we regained the ability to tune the resonant response of the metamaterial within the previously established limits of the transmission level (43−30%) and bias voltage (0−6.5 V), although this time in a continuous and reversible manner. In particular, when we ramped the voltage up, the level of transmission decreased more gradually, without a sharp drop characteristic of the onset of stiction (see Figure 3d). The change of the metamaterial response was complete at 6.5 V with no further modifications of the spectrum visible at higher voltage (increasing the voltage past 7 V often led to electrical breakdown of the samples). However, contrary to the previous scenarios (involving isotropic LC or no LC), the transparency of the sample was also seen to recover during the

voltage ramp-down, as soon as the potential difference dropped below 6.5 V. Figure 3d shows that the trends of the transmission change measured with increasing and decreasing bias voltage overlapped except for the very first ramp-up—ramp-down cycle, when a slight hysteresis was observed.

Remarkably, by cycling the phase of the LC between nematic and isotropic we were able to toggle between reversible (Figure 3b) and irreversible (Figure 3d) regimes of controlling metamaterial transmission.

While irreversible switching of an LC-infiltrated sample was a clear manifestation of NEMS stiction, the discovered regime of its reversible operation must have also engaged actuations of the nanobridges, which were somewhat immune to stiction. Indeed, according to our simulations (see the Supporting Information), the reorientation of the nematic director in the bulk of the LC layer and the corresponding changes of optical anisotropy would have occurred below 3.0 V. Also, the measured overall change of the metamaterial transmission in the presence of a nematic and isotropic LC had the same magnitude, which together with the simulation results rules out electrically controlled birefringence as the only mechanism for the observed transmission variation. Besides, toggling between reversible and irreversible regimes of metamaterial optical switching could be possible only if the nanobridges became unstuck upon cooling the sample and were free to move while the LC remained in the nematic phase. The behavior of metamaterial transmission around 6.5 V (Figure 3b and d) suggests that the magnitude of the structural deformation at the end of the voltage ramp-up reached the physically allowed limit, where every other gap between the nanobridges had closed up. That brought the nanobridges within the effective range of the surface adhesion forces and should have resulted in stiction, just as it occurred while the LC was in the isotropic phase. Below we discuss possible mechanisms of the stiction suppression, deferring an in-depth quantitative analysis of the effect to a future publication.

The main failure mode of electrostatically driven actuators and capacitive switches that is related to stiction is dielectric charging.[36,37] The reduction of parasitic, electrostatic attraction between silicon nitride nanobridges (which are charged to at least 6.5 V upon irreversible switching) is therefore one of the likely causes of the observed stiction-free behavior. In particular, one may expect the attraction force F_{att} to decrease as the result of a change of the local dielectric permittivity ε during the transition of LC to the nematic state. In this case the permittivity of the LC becomes highly anisotropic, while the residual electric field between the nanobridges is strong enough to deform the LC director locally and orient most of the LC molecules along the field lines.[38,39] The switching of the LC phase from isotropic to nematic is thus accompanied by an increase of the static dielectric constant in the vicinity of the closed gaps and, given that $F_{att} \propto 1/\varepsilon$ for electrically isolated charged bodies, can in principle trigger the release of the nanobridges at zero bias. However, this mechanism of stiction suppression no longer applies during the actuation of the nanobridges, when the metamaterial wire grid is connected to a voltage source. In this case $F_{att} \propto \varepsilon$, so at the end of voltage ramp-up the electrostatic attraction mediated by the nematic phase of the LC turns out to be even stronger than in the case of the isotropic LC (which is also supported by the results of our simulations, presented in the Supporting Information). It cannot be counteracted by the London dispersion forces, since for a symmetric configuration (such as a pair of silicon nitride

boundaries separated by a dielectric layer) they were shown to be always attractive.[40,41] We also rule out electric discharge as an antistiction mechanism specific to the nematic phase; it would involve localized heating and hence result in distortions of the LC, which could be easily observed under a polarized optical microscope in the course of our measurements; besides, ion mobility in the nematic phase is generally lower than in the isotropic one.[42]

We therefore conclude that stiction-free switching of the reconfigurable metamaterial resulted from an increase of the mechanical restoring force, which must have acquired a contribution from elastic distortions of LC. For example, the electric field between closing nanobridges (>10 kV/mm) may cause a substantial increase of LC viscosity near the gap[43,44] and suppress the flow coupling, which will locally render the nematic LC as an elastomer that counteracts the adhesion forces through electrically induced splay and/or bend deformations. Distortions of the nematic director also lead to the appearance of the so-called structural forces.[45−47] Being the consequence of the long-range orientational order and orientational elasticity of a nematic LC,[47] the structural forces can affect actuations of the nanobridges within the entire range of physically allowed displacements and, hence, may even underpin the more gradual trend of the transmission change observed during the reversible switching (Figure 3d). While stiction-free switching has been demonstrated with 5CB, a standard and well-characterized in the literature nematic liquid crystal, a similar behavior is expected with other liquid crystals from the same class, such as, E7 and TL205.

CONCLUSIONS

By infiltrating a NEMS-based reconfigurable metasurface with a nematic liquid crystal we were able to prevent permanent adhesion between movable parts of the nanostructure occurring in the course of its mechanical switching. Apart from being a more straightforward and easy-to-implement alternative to the existing antistiction solutions, our approach also introduces an active mechanism of stiction control, which enables a fully reversible transition from stiction-free back to the usual (stiction-limited) regime of NEMS operation. The mechanism exploits coupling between mechanical deformations of the nanoactuators and elastic distortions of LC molecular structure arising in ordered LC phases. It is expected to greatly expand the functionality of NEMS/MEMS devices, given high susceptibility of liquid crystals to a wide range of external stimuli including heat, light, and electric and magnetic fields.[48] In particular, controlled stiction could be exploited in nonvolatile memory or field-programmable gate arrays based on NEMS. Elasto-mechanical coupling brings together intrinsic nonlinearity of liquid crystals and dynamic tuneability of the reconfigurable metamaterials, opening a route toward, for example, the realization of magneto-elastic metamaterials[49] at optical frequencies. Also, a broad spectrum of structural transitions exhibited by liquid crystals at the nanoscale (which includes most notably positional and orientational ordering,[50] nematic capillary condensation,[51,52] and presmectic layering[53,54]) should enrich the switching behavior of LC-infiltrated electro-mechanical actuators and reconfigurable meta-devices[55] near the LC clearing point, thus making the latter a practical proposition for developing adaptive and "smart" nanosystems.

METHODS

Sample Fabrication. The design of a mechanically reconfigurable metasurface was based on a double-periodic array of electrically connected V-shaped plasmonic nano-resonators forming a continuous "zigzag" wire pattern (see Figure 1b). The metasurface was fabricated by milling, with a focused ion beam, a 60 nm thick gold film that had been sputtered beforehand on a 50 nm thick ultra-low-stress silicon nitride membrane (Norcada). The resulting gold wires had a width of approximately 160 nm and were separated by 100 nm wide gaps. The unit cell of the zigzag pattern was rectangular with a size of 340 nm × 490 nm, which rendered our planar metamaterial as nondiffracting in the visible and near-IR, at wavelengths larger than 0.5 μm. The milling also completely removed parts of the membrane in the gaps between the nanowires, thus yielding a gold zigzag grid fully suspended on silicon nitride nanobridges (Figure 1c). The zigzag sections of the metasurface also received 2 μm long straight extensions at both ends, which helped to reduce the stiffness of the metamaterial structure. The nanowires were grouped into pairs with the odd and even pairs being electrically disconnected from the opposite sections of the remaining gold film (Figure 1d), which had been split to act as macroscopic dc voltage terminals (as illustrated in Figure 1a). The overall size of the reconfigurable metasurface was 13 μm × 17 μm.

Infiltration with a Liquid Crystal. The metamaterial was infiltrated with the nematic liquid crystal 5CB (Merck). Our choice was dictated merely by the convenience of working with 5CB, which has the lowest clearing temperature among widely available nematic liquid crystals (35 °C), relatively low viscosity, and weak optical anisotropy ($n_o = 1.520$, $n_e = 1.681$, $n_{iso} = 1.574$ at $\lambda = 1$ μm).[56] 5CB was applied to the surface of the sample using a drop-casting method (see illustration in Figure 1a). To facilitate optical measurements, the drop was squeezed by a glass cover slide, yielding a thin, optically uniform LC layer. The glass slide was coated with a 20 nm thick film of unrubbed polyimide, which ensured both parallel alignment and weak anchoring of LC molecules at its surface. The thickness of the LC layer was set to 2 μm by dielectric spacers placed between the glass cover and gold film. To promote the infiltration, we maintained the temperature of the sample above the clearing point of 5CB for about 10 min.

Optical Measurements. Optical response of the meta-material sample was characterized in transmission at normal incidence using linearly polarized light. The polarization was set parallel to the nanowires of the zigzag pattern. Transmission spectra were collected in the range 0.7–1.9 μm with a spectral resolution of 0.1 μm using a microscope connected to a spectrometer.

ASSOCIATED CONTENT

ⓢ Supporting Information

The Supporting Information is available free of charge on the ACS Publications website at DOI: 10.1021/acsnano.6b07495.

> Modeling changes in the optical anisotropy of an LC layer and distribution of the control electric field (PDF)
> Videos of a pristine reconfigurable metasurface made under SEM while ramping the control voltage up and down (XviD/AVI) (AVI)
> (AVI)

AUTHOR INFORMATION

Corresponding Author
*E-mail (V. A. Fedotov): vaf@orc.soton.ac.uk.

ORCID ⓞ
Vassili A. Fedotov: 0000-0003-4862-574X

Notes
The authors declare no competing financial interest.

REFERENCES

(1) Ekinci, K. L.; Roukes, M. L. Nanoelectromechanical Systems. *Rev. Sci. Instrum.* **2005**, *76*, 061101.
(2) Im, H.; Huang, X.-J.; Gu, B.; Choi, Y.-K. A Dielectric-Modulated Field-Effect Transistor for Biosensing. *Nat. Nanotechnol.* **2007**, *2*, 430–434.
(3) Naik, A. K.; Hanay, M. S.; Hiebert, W. K.; Feng, X. L.; Roukes, X. L. Towards Single-Molecule Nanomechanical Mass Spectrometry. *Nat. Nanotechnol.* **2009**, *4*, 445–450.
(4) Bagci, T.; Simonsen, A.; Schmid, S.; Villanueva, L. G.; Zeuthen, E.; Appel, J.; Taylor, J. M.; Srensen, A.; Usami, K.; Schliesser, A.; Polzik, E. S. Optical Detection of Radio Waves Through a Nanomechanical Transducer. *Nature* **2014**, *507*, 81–85.
(5) Akram, U.; Kiesel, N.; Aspelmeyer, M.; Milburn, G. J. Single-Photon Opto-Mechanics in the Strong Coupling Regime. *New J. Phys.* **2010**, *12*, 083030.
(6) Verhagen, E.; Deléglise, S.; Weis, S.; Schliesser, A.; Kippenberg, T. J. Quantum-Coherent Coupling of a Mechanical Oscillator to an Optical Cavity Mode. *Nature* **2012**, *482*, 63–67.
(7) Lee, S. W.; Lee, D. S.; Morjan, R. E.; Jhang, S. H.; Sveningsson, M.; Nerushev, O. A.; Park, Y. W.; Campbell, E. E. B. A Three-Terminal Carbon Nanorelay. *Nano Lett.* **2004**, *4*, 2027–2030.
(8) Jang, W. W.; Lee, J. O.; Yoon, J.-B.; Kim, M.-S.; Lee, J.-M.; Kim, S.-M.; Cho, K.-H.; Kim, D.-W.; Park, D.; Lee, W.-S. Fabrication and Characterization of a Nanoelectromechanical Switch with 15-nm-Thick Suspension Air Gap. *Appl. Phys. Lett.* **2008**, *92*, 103110.
(9) Loh, O. Y.; Espinosa, H. D. Nanoelectromechanical Contact Switches,. *Nat. Nanotechnol.* **2012**, *7*, 283–295.
(10) Jang, J. E.; Cha, S. N.; Choi, Y. J.; Kang, D. J.; Butler, T. P.; Hasko, D. G.; Jung, J. E.; Kim, J. M.; Amaratunga, G. A. J. Nanoscale Memory Cell Based on a Nanoelectromechanical Switched Capacitor. *Nat. Nanotechnol.* **2008**, *3*, 26–30.
(11) Rueckes, T.; Kim, K.; Joselevich, E.; Tseng, G. Y.; Cheung, C.-L.; Lieber, C. M. Carbon Nanotube-Based Nonvolatile Random Access Memory for Molecular Computing. *Science* **2000**, *289*, 94–97.
(12) Lee, S. W.; Park, S. J.; Campbell, E. E.; Park, Y. A Fast and Low-Power Microelectromechanical System-Based Non-Volatile Memory Device. *Nat. Commun.* **2011**, *2*, 220.
(13) Ou, J. Y.; Plum, E.; Zhang, J.; Zheludev, N. I. An Electromechanically Reconfigurable Plasmonic Metamaterial Operating in the Near-Infrared. *Nat. Nanotechnol.* **2013**, *8*, 252–255.
(14) Yamaguchi, K.; Fujii, M.; Okamoto, T.; Haraguchi, M. Electrically Driven Plasmon Chip: Active Plasmon Filter. *Appl. Phys. Express* **2014**, *7*, 012201.
(15) Thijssen, R.; Verhagen, E.; Kippenberg, T. J.; Polman, A. Plasmon Nanomechanical Coupling for Nanoscale Transduction. *Nano Lett.* **2013**, *13*, 3293–3297.

(16) Liu, X.; Padilla, W. J. Dynamic Manipulation of Infrared Radiation with MEMS Metamaterials. *Adv. Opt. Mater.* **2013**, *1*, 559−562.

(17) Yamaguchi, K.; Yamanaka, H.; Ohtsu, T.; Ishii, S. Electrically Driven Plasmon Chip: Active Plasmon Lens in the Visible Range. *Appl. Phys. Lett.* **2016**, *108*, 111903.

(18) Maboudian, R.; Howe, R. T. Critical Review: Adhesion in Surface Micromechanical Structures. *J. Vac. Sci. Technol., B: Microelectron. Process. Phenom.* **1997**, *B15*, 1−20.

(19) Yapu, Z. Stiction and Anti-Stiction in MEMS and NEMS. *Acta Mech. Sin.* **2003**, *19*, 1−10.

(20) Guckel, H.; Sniegowski, J. J.; Christenson, T. R.; Raissi, F. The Application of Fine Grained, Tensile Polysilicon Mechanically Resonant Transducers. *Sens. Actuators, A* **1990**, *A21-A23*, 346−51.

(21) Maboudian, R. Surface Processes in MEMS Technology. *Surf. Sci. Rep.* **1998**, *30*, 207−269.

(22) Maboudian, R.; Ashurst, W. R.; Carraro, C. Tribological challenges in micromechanical systems. *Tribol. Lett.* **2002**, *12*, 95−100.

(23) Mastrangelo, C. H. Adhesion-Related Failure Mechanisms in Micromechanical Devices. *Tribol. Lett.* **1997**, *3*, 223−238.

(24) de Boer, M. P.; Mayer, T. M. Tribology of MEMS. *MRS Bull.* **2001**, *26*, 302−304.

(25) Maboudian, R.; Ashurst, W. R.; Carraro, C. Self-Assembled Monolayers as Anti-Stiction Coatings for MEMS: Characteristics and Recent Developments. *Sens. Actuators, A* **2000**, *82*, 219−223.

(26) Mercado, L. L.; Kuo, S.-M.; Lee, T.-Y. T.; Liu, L. Mechanics-Based Solutions to RF MEMS Switch Stiction Problem. *IEEE Trans. Compon. Packag. Technol.* **2004**, *27*, 560−567.

(27) Lee, J. O.; Song, Y.-H.; Kim, M.-W.; Kang, M.-H.; Oh, J.-S.; Yang, H.-H.; Yoon, J.-B. A Sub-1-V Nanoelectromechanical Switching Device. *Nat. Nanotechnol.* **2013**, *8*, 36−40.

(28) Romig, A. D., Jr.; Dugger, M. T.; McWhorter, P. J. Materials Issues in Microelectromechanical Devices: Science, Engineering, Manufacturability and Reliability. *Acta Mater.* **2003**, *51*, 5837−5866.

(29) Scharf, T. W.; Prasad, S. V.; Dugger, M. T.; Kotula, P. G.; Goeke, R. S.; Grubbs, R. K. Growth, Structure, and Tribological Behavior of Atomic Layer-Deposited Tungsten Disulphide Solid Lubricant Coatings with Applications to MEMS. *Acta Mater.* **2006**, *54*, 4731−4743.

(30) Asay, D. B.; Dugger, M. T.; Kim, S. H. *In Situ* Vapor-Phase Lubrication of MEMS. *Tribol. Lett.* **2008**, *29*, 67−74.

(31) Ashurst, W. R.; Carraro, C.; Maboudian, R. Vapor Phase Anti-Stiction Coatings for MEMS. *IEEE Trans. Device Mater. Reliab.* **2003**, *3*, 173−178.

(32) Zheludev, N. I.; Plum, E. Reconfigurable Nanomechanical Photonic Metamaterials. *Nat. Nanotechnol.* **2016**, *11*, 16−22.

(33) Buchnev, O.; Ou, J. Y.; Kaczmarek, M.; Zheludev, N. I.; Fedotov, V. A. Electro-Optical Control in a Plasmonic Metamaterial Hybridised with a Liquid-Crystal Cell. *Opt. Express* **2013**, *21*, 1633−1638.

(34) Buchnev, O.; Podoliak, N.; Kaczmarek, M.; Zheludev, N. I.; Fedotov, V. A. Electrically Controlled Nanostructured Metasurface Loaded with Liquid Crystal: Toward Multifunctional Photonic Switch. *Adv. Opt. Mater.* **2015**, *3*, 674−679.

(35) Valente, J.; Ou, J. Y.; Plum, E.; Youngs, I. J.; Zheludev, N. I. A Magneto-Electro-Optical Effect in a Plasmonic Nanowire Material. *Nat. Commun.* **2015**, *6*, 7021.

(36) Wibbeler, J.; Pfeifer, G.; Hietschold, M. Parasitic Charging of Dielectric Surfaces in Capacitive Microelectromechanical Systems (MEMS). *Sens. Actuators, A* **1998**, *A71*, 74−80.

(37) Zaghloul, U.; Papaioannou, G. J.; Coccetti, F.; Pons, P.; Plana, R. A Systematic Reliability Investigation of the Dielectric Charging Process in Electrostatically Actuated MEMS Based on Kelvin Probe Force Microscopy. *J. Micromech. Microeng.* **2010**, *20*, 064016.

(38) Self, R. H.; Please, C. P.; Sluckin, T. J. Deformation of Nematic Liquid Crystals in an Electric Field. *Eur. J. Appl. Math.* **2002**, *13*, 1−23.

(39) Gorkunov, M. V.; Osipov, M. A. Tunability of Wire-Grid Metamaterial Immersed into Nematic Liquid Crystal. *J. Appl. Phys.* **2008**, *103*, 036101.

(40) French, R. H.; Mullejans, H.; Jones, D. J.; Duscher, G.; Cannon, R. M.; Ruhle, M. Dispersion Forces and Hamaker Constants for Intergranular Film in Silicon Nitride from Spatially Resolved Valence Electron Energy Loss Spectrum Imaging. *Acta Mater.* **1998**, *46*, 2271−2287.

(41) French, R. H. Origins and Applications of London Dispersion Forces and Hamaker Constants in Ceramics. *J. Am. Ceram. Soc.* **2000**, *83*, 2117−2146.

(42) Derfela, G.; Lipiński, A. Charge Carrier Mobility Measurements in Nematic Liquid Crystals. *Mol. Cryst. Liq. Cryst.* **1979**, *55*, 89−100.

(43) Tani, J.; Takagi, T.; Nakaniwa, H.; Ohtomo, K.; Kosugo, K. Vibration Suppression Effect of Liquid Crystal under Electromagnetic Field. *J. Intell. Mater. Syst. Struct.* **1996**, *3*, 272−277.

(44) Morishita, S.; Nakano, K.; Kimura, Y. Electroviscous Effect of Nematic Liquid Crystals. *Tribol. Int.* **1993**, *26*, 399−403.

(45) Horn, R. G.; Israelachvili, J. N. Direct Measurement of Structural Forces Between 2 Surfaces in a Non-Polar Liquid. *J. Chem. Phys.* **1981**, *75*, 1400−1411.

(46) Poulin, P.; Stark, H.; Lubensky, T. C.; Weitz, D. A. Novel Colloidal Interactions in Anisotropic Fluids. *Science* **1997**, *275*, 1770−1773.

(47) Musevic, I. Forces in Nematic Liquid Crystals: from Nanoscale Interfacial Forces to Long-Range Forces in Nematic Colloids. *Liq. Cryst.* **2009**, *36*, 639−647.

(48) de Gennes, P. G.; Prost, J. *The Physics of Liquid Crystals*; Oxford University Press, 1995.

(49) Lapine, M.; Shadrivov, I. V.; Powell, D. A.; Kivshar, Y. S. Magnetoelastic Metamaterials. *Nat. Mater.* **2012**, *11*, 30−33.

(50) Ruths, M.; Steinberg, S.; Israelachvili, J. N. Effects of Confinement and Shear on the Properties of Thin Films of Thermotropic Liquid Crystal. *Langmuir* **1996**, *12*, 6637−6650.

(51) Poniewierski, A.; Sluckin, T. J. Theory of the Nematic-Isotropic Transition in a Restricted Geometry. *Liq. Cryst.* **1987**, *2*, 281−311.

(52) Kocevar, K.; Borstnik, A.; Musevic, I.; Zumer, S. Capillary Condensation of a Nematic Liquid Crystal Observed by Force Spectroscopy. *Phys. Rev. Lett.* **2001**, *86*, 5914−5917.

(53) de Gennes, P. G. Interactions Between Solid Surfaces in a Presmestic Fluid. *Langmuir* **1990**, *6*, 1448−1450.

(54) Ziherl, P. Structural Force in a Presmectic Liquid. *Phys. Rev. E: Stat. Phys., Plasmas, Fluids, Relat. Interdiscip. Top.* **2000**, *61*, 4636−4639.

(55) Zheludev, N. I.; Kivshar, Y. S. From Metamaterials to Metadevices. *Nat. Mater.* **2012**, *11*, 917−924.

(56) Li, J.; Wen, C.-H.; Gauza, S.; Lu, R.; Wu, S.-T. Refractive Indices of Liquid Crystals for Display Applications. *J. Disp. Technol.* **2005**, *1*, 51−61.